Available online at www.sciencedirect.com
ScienceDirect
Journal of Sound and Vibration 315 (2008) 1103–1124
JOURNAL OF SOUND AND VIBRATION
www.elsevier.com/locate/jsvi

A computational mode-matching approach for sound propagation in three-dimensional ducts with flow

G. Gabard*, R.J. Astley

Institute of Sound and Vibration Research, University of Southampton, Southampton SO17 1BJ, UK

Received 3 August 2007; received in revised form 7 February 2008; accepted 12 February 2008
Handling Editor: C. Morfey
Available online 28 March 2008

Abstract

A finite element (FE) mode-matching approach is presented for duct acoustics with flow and circumferentially varying liners. The primary application of the method is the prediction of sound attenuation in turbofan inlets and bypass ducts including the effects of liner splices. A fully numerical procedure has been developed to determine the acoustic modes in ducts of arbitrary cross-section and mean flow profile. A numerical mode-matching method is proposed using a modified matching technique in order to deal more accurately with liner discontinuity with flow. An analytic radiation model can also be integrated with the mode-matching procedure in order to obtain far-field directivity for tones and broadband multimode noise. The accuracy of the mode-matching method is demonstrated by comparison with exact solutions and high-resolution FE solutions. The influence of non-axisymmetric liners on noise radiation is also illustrated.

1. Introduction

A numerical mode-matching procedure is applied to the acoustic analysis of turbofan intakes and bypass ducts and is coupled to an analytic radiation model to predict the effect of non-uniform liners on far-field radiation. The present method features an improved matching condition which is able to describe accurately sound scattering by liner discontinuities with flow. A general numerical scheme is used to compute the eigenmodes in each duct segment, which makes the method applicable to ducts of arbitrary cross-section and with peripherally varying liners.

The expansion of the sound field in terms of modes forms the basis for many analytic and semi-analytic methods in duct acoustics. This has many attractive features and leads to an immediate reduction in the dimension of the problem in that the acoustic field in a prismatic two-dimensional (2-D) or axisymmetric duct can be decomposed into modal solutions of a one-dimensional (1-D) eigenvalue problem, and similarly wave fields in a duct of arbitrary cross-section can be expanded in terms of eigenvectors defined over a 2-D duct cross-section. By matching expansions of this type at the interface between different uniform duct segments, the effect of axial variations of impedance can be modelled with far fewer parameters than would be required

*Corresponding author.
E-mail addresses: gabard@soton.ac.uk (G. Gabard), rja@isvr.soton.ac.uk (R.J. Astley).

0022-460X/$ - see front matter © 2008 Elsevier Ltd. All rights reserved.
doi:10.1016/j.jsv.2008.02.015

for a three-dimensional (3-D) numerical transmission analysis [1]. The downside of such an approach is that when flow is present, it can be applied only to prismatic ducts, i.e. ducts whose cross-sectional geometry is uniform in the axial direction. Moreover, analytic solutions are only readily available for special geometries and flow conditions: circular, annular and rectangular ducts with uniform mean flow and liners which are uniform in the circumferential or transverse directions. For circular and annular ducts with circumferentially varying liner impedances, semi-analytic methods have been proposed for the duct eigenvalue problem by using a Fourier expansion of the impedance [2,3], but these have not been demonstrated to be effective for the high frequencies and mode orders which are typical of turbofan duct applications. A semi-analytic multimode propagation method has also been developed which uses a rigid duct modal basis and which reduces the transmission problem to the solution of a set of modal ordinary differential equations along the duct. This has recently been applied to the case of a circular duct with peripherally varying liners in the absence of flow [4].

The determination of the lined acoustic modes, even for ducts of separable geometry, is a non-trivial exercise, particularly when flow is present. 'Surface' modes exist for particular ranges of wall impedance, and the development of robust methods which are able to resolve *all* of the modes *all* of the time is not a simple matter [5]. When the mean flow in the duct is non-uniform the task becomes more difficult and some form of numerical procedure must be used, either to solve an eigenvalue relationship numerically, or to solve directly an equivalent discrete problem. In the latter instance, a finite element (FE) representation of the duct cross-section is an obvious choice [6].

FE models for calculating the eigenmodes in ducts of arbitrary cross-section and with peripherally varying liners were first proposed in the early 1980s [7]. These were based on the linearized Euler equations. Their application was limited to low frequencies and coarse meshes by the computational resources available at that time. In the current article this general approach is revisited. A weak form of the convected wave equation forms the basis for the current FE eigenvalue formulation. It is found that complete sets of propagating eigenmodes can be obtained at modest computational cost for frequencies and flow conditions which are characteristic of turbofan intake and bypass ducts. This approach is presented in Section 2 of the current article.

In Section 3, a new Galerkin mode-matching procedure is proposed which deals correctly with axial impedance discontinuities. This method is coupled to an analytic radiation model in Section 4, and in Section 5 it is applied to the prediction of scattering and attenuation in lined duct segments with peripherally varying impedances. In particular, the method is used to assess the effect of liner length and liner-splice thickness on turbofan intake and bypass ducts in which hard axial splices are present.

The use of a modal representation within the duct lends itself also to integration with analytic radiation models at the duct exit. As shown in Section 4, it is then possible to characterize the influence of the liners in terms of the sound radiated to the far field.

2. The FE eigenvalue problem

A fully numerical procedure has been developed to determine the acoustic modes in ducts of arbitrary cross-section and mean flow profile. The starting point for the formulation is a weak variational statement of the Pridmore-Brown equation written for ducts of arbitrary cross-section and carrying a parallel subsonic mean flow of arbitrary profile. An FE method is then devised to solve the eigenvalue problem.

2.1. Formulation of the eigenvalue problem

Consider a prismatic duct with axis z and cross-section S, see Fig. 1. The formulation of the eigenvalue problem and its FE implementation is presented for the general case of a sheared flow in which the axial flow velocity w_0 varies with the transverse coordinates x and y, i.e. $w_0 = w_0(x, y)$ (results will be presented in this article only for the case of an axial mean flow w_0 which is constant across the duct). The flow is assumed to be adiabatic and isentropic and of uniform temperature, so that the mean sound speed c_0 and density ρ_0 are constant over the duct. It is not difficult to show that in such circumstances, the complex amplitude of the

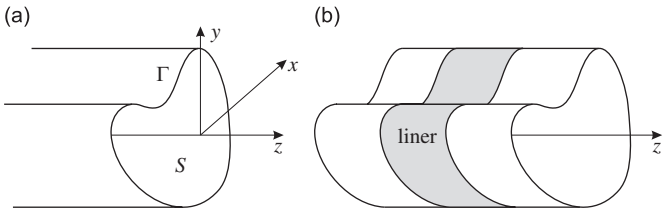

Fig. 1. (a) Schematic of the prismatic duct with axis z and cross-section S and (b) schematic of the segmented duct composed of several axial segments.

pressure perturbation in the duct, $p(x,y,z)$ satisfies Pridmore-Brown's equation

$$\left(\mathrm{i}\omega + w_0\frac{\partial}{\partial z}\right)\left[\frac{1}{c_0^2}\left(\mathrm{i}\omega + w_0\frac{\partial}{\partial z}\right)^2 p - \Delta p\right] + 2\frac{\partial}{\partial z}(\nabla_\perp w_0 \cdot \nabla_\perp p) = 0, \tag{1}$$

where $\nabla_\perp$ is the gradient operator in the cross-section of the duct. In the case of uniform flow, the last term is zero, and the above equation reduces to the convected wave equation:

$$\frac{1}{c_0^2}\left(\mathrm{i}\omega + w_0\frac{\partial}{\partial z}\right)^2 p - \Delta p = 0.$$

In either event, the Myers boundary condition is applied at the duct walls:

$$\frac{\partial p}{\partial n} = \frac{\rho_0}{-\mathrm{i}\omega Z}\left(\mathrm{i}\omega + w_0\frac{\partial}{\partial z}\right)^2 p, \tag{2}$$

where Z is the wall impedance which can vary arbitrarily around the duct wall but which is uniform in the axial direction. Solutions are now sought of the form

$$p(x,y,z) \equiv P(x,y)\mathrm{e}^{-\mathrm{i}k\lambda z},$$

where $k = \omega/c_0$ is the free-field wavenumber and $k\lambda = k_z$ is the axial wavenumber of the mode. Eq. (1) can then be written

$$(1-\lambda M_0)[\Delta_\perp P + k^2[(1-M_0\lambda)^2 - \lambda^2]P] + 2\lambda[\nabla_\perp M_0 \cdot \nabla_\perp P] = 0 \quad \text{with } \Delta_\perp \equiv \frac{\partial}{\partial x^2} + \frac{\partial}{\partial y^2}, \tag{3}$$

where $M_0 = w_0/c_0$ is the flow Mach number. From the boundary condition (2), one gets

$$\frac{\partial P}{\partial n} = \frac{\rho_0 c_0 k}{\mathrm{i}Z}(1-M_0\lambda)^2 P. \tag{4}$$

Eqs. (3) and (4) represent an eigenvalue problem defined on the duct cross-section S with eigenvalue λ and eigenvector P. In order to obtain numerical approximations of this eigenvalue problem, it is recast as a variational formulation

$$\int_S [(1-\lambda M_0)[k^2\overline{W}[(1-M_0\lambda)^2 - \lambda^2]P - \nabla_\perp\overline{W}\cdot\nabla_\perp P] + 3\lambda\overline{W}\nabla_\perp M_0\cdot\nabla_\perp P]\,\mathrm{d}S + \oint_\Gamma \overline{W}\frac{\rho_0 c_0 k}{\mathrm{i}Z}(1-M_0\lambda)^3 P\,\mathrm{d}\Gamma = 0, \quad \forall W, \tag{5}$$

where W is a trial function and $\Gamma = \partial S$ is the boundary of S. The overbar denotes the complex conjugate.

2.2. The discrete problem

The variational formulation is discretized by applying the FE method. The duct cross-section S is approximated by a mesh of FEs (examples are given in Fig. 2). The mode shape P and the trial function W are

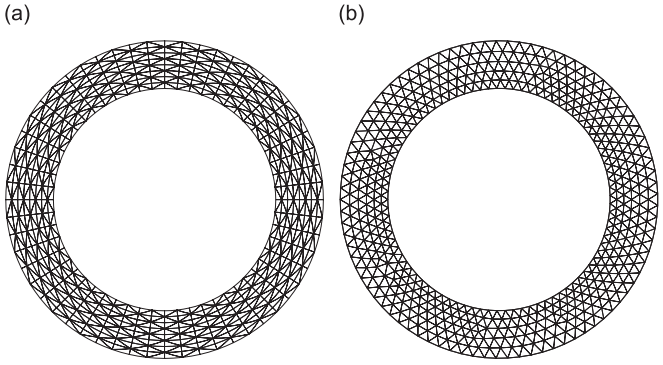

Fig. 2. Examples of finite element meshes used for the validation of the eigenvalue problem. (a) Structured mesh; (b) Unstructured mesh.

interpolated on the mesh:

$$P(x,y) = \mathbf{N}(x,y)\mathbf{p}_n, \quad W(x,y) = \mathbf{N}(x,y)\mathbf{w}_n, \tag{6}$$

where $\mathbf{N}$ is a row vector containing the global interpolation functions and $\mathbf{p}_n$ and $\mathbf{w}_n$ are the vectors of the nodal values of P and W, respectively. It is convenient before proceeding further to define Mach weighted acoustic 'mass', 'stiffness' and 'boundary impedance' matrices for the duct cross-section and its boundary. These are given by

$$\mathbf{M}^{(n)} = \int_S (M_0)^n [\mathbf{N}^{\mathrm{T}}\mathbf{N}]\,\mathrm{d}S, \quad \mathbf{K}^{(n)} = \int_S (M_0)^n \left[\frac{\partial \mathbf{N}^{\mathrm{T}}}{\partial x}\frac{\partial \mathbf{N}}{\partial x} + \frac{\partial \mathbf{N}^{\mathrm{T}}}{\partial y}\frac{\partial \mathbf{N}}{\partial y}\right] \mathrm{d}S,$$

$$\mathbf{Z}^{(n)} = \int_\Gamma \frac{\rho_0 c_0 k}{\mathrm{i}Z}(M_0)^n [\mathbf{N}^{\mathrm{T}}\mathbf{N}]\,\mathrm{d}S,$$

for $n = 0, 1, 2, 3$. For the case of uniform mean flow $M_0(x,y) = M_0$ (const.) each of these matrices satisfies the identity: $[]^{(n)} \equiv M_0^n[]^{(0)}$. When non-uniform flow is present we must define also a shear coupling matrix $\mathbf{S}$ given by

$$\mathbf{S} = \int_S \left[\mathbf{N}^{\mathrm{T}}\left(\frac{\partial M_0}{\partial x}\frac{\partial \mathbf{N}}{\partial x} + \frac{\partial M_0}{\partial y}\frac{\partial \mathbf{N}}{\partial y}\right)\right] \mathrm{d}S.$$

This is zero for the case of uniform flow. When expressions (6) are substituted into the variational statement (5) we obtain an algebraic eigenvalue problem for λ of the form

$$(\mathbf{A}_0 + \lambda\mathbf{A}_1 + \lambda^2\mathbf{A}_2 + \lambda^3\mathbf{A}_3)\mathbf{p}_n = \mathbf{0}, \tag{7}$$

where $\mathbf{A}_0, \ldots, \mathbf{A}_3$ are constant $n \times n$ matrices:

$$\mathbf{A}_0 = k^2\mathbf{M}^{(0)} - \mathbf{K}^{(0)} + \mathbf{Z}^{(0)},$$

$$\mathbf{A}_1 = -3k^2\mathbf{M}^{(1)} + \mathbf{K}^{(1)} - 3\mathbf{Z}^{(1)} + 3\mathbf{S},$$

$$\mathbf{A}_2 = k^2(3\mathbf{M}^{(2)} - \mathbf{M}^{(0)}) + 3\mathbf{Z}^{(2)},$$

$$\mathbf{A}_3 = -k^2(\mathbf{M}^{(3)} + \mathbf{M}^{(1)}) - \mathbf{Z}^{(3)}.$$

Eq. (7) can be re-written as a linear eigenvalue problem in λ of dimension $3n \times 3n$ and solved numerically to give $3n$ eigenvalues and eigenvectors. These include both acoustic and hydrodynamic modes.[1] Some simplification is possible when the mean flow is uniform or zero.

[1]When sheared flow is present there is no clear distinction between acoustic and vortical modes but some eigensolutions are predominantly irrotational and acoustic in nature while some are predominantly rotational and convected with the mean flow.

In the case of zero mean flow, $M_0(x,y) \equiv 0$, the discrete eigenproblem (7) reduces to a linear eigenproblem in λ^2:

$$(\mathbf{B}_0 + \lambda^2 \mathbf{B}_2)\mathbf{p}_n = \mathbf{0}, \tag{8}$$

where

$$\mathbf{B}_0 = k^2\mathbf{M}^{(0)} + \mathbf{Z}^{(0)} - \mathbf{K}^{(0)} \quad \text{and} \quad \mathbf{B}_2 = -k^2\mathbf{M}^{(0)}.$$

This has n eigensolutions giving axial wavenumbers λ which occur in conjugate pairs corresponding to upstream and downstream propagating modes.

When the mean flow is non-zero but uniform, $M_0(x,y) \equiv M_0$ constant, a factor $(1 - \lambda M_0)$ can be removed from Eq. (7) to give a modified expression:

$$(1 - \lambda M_0)(\mathbf{C}_0 + \lambda \mathbf{C}_1 + \lambda^2 \mathbf{C}_2)\mathbf{p}_n = \mathbf{0},$$

where the matrices $\mathbf{C}_n$ $(n = 0, 1, 2)$ are given by

$$\mathbf{C}_0 = k^2\mathbf{M}^{(0)} - \mathbf{K}^{(0)} + \mathbf{Z}^{(0)},$$

$$\mathbf{C}_1 = -2M_0(k^2\mathbf{M}^{(0)} + \mathbf{Z}^{(0)}),$$

$$\mathbf{C}_2 = k^2(M_0^2 - 1)\mathbf{M}^{(0)} + M_0^2\mathbf{Z}^{(0)}.$$

The factor $(1 - M_0\lambda)$ gives multiple roots $\lambda = 1/M_0$, which correspond to hydrodynamic disturbances which are convected with the mean flow. The acoustic modes are then obtained from the remaining factor, i.e. by solving

$$(\mathbf{C}_0 + \lambda \mathbf{C}_1 + \lambda^2 \mathbf{C}_2)\mathbf{p}_n = \mathbf{0}. \tag{9}$$

The algebraic eigenvalue problem defined by Eq. (7) and the special cases (8) and (9) are solved as linear matrix eigenvalue problems in λ or λ^2. The implicitly restarted Arnoldi method is used as implemented in the ARPACK solver designed and optimized for large-scale sparse eigenvalue problems [8].

2.3. Ordering of the eigensolutions

Formulation (5) based on Eq. (3) does not make any distinction between modes propagating in the positive and negative axial directions. But for the mode-matching method described below, it is important to distinguish the positive modes from the negative ones. For acoustic modes, this is done using two properties of the modes. The first argument is that the amplitude of the acoustic perturbations should decrease away from the source. Therefore, the sign of $\mathrm{Im}(k_z)$ indicates the direction of propagation of the mode: $\mathrm{Im}(k_z) < 0$ for positive modes and $\mathrm{Im}(k_z) > 0$ for negative modes. For modes with real wavenumbers, the direction of the power flux indicates the direction of propagation. The axial power flux generated by a single mode is the following:

$$P = \frac{\rho_0\omega^2}{2c_0}\left[(1 - M_0^2)\frac{k_z}{k} + M_0\right]\int_S |P(x,y)|^2 \,\mathrm{d}S.$$

Therefore the propagation direction is given by the term in brackets and a mode is propagating in the positive direction if $k_z > -kM_0/(1 - M_0^2)$.

The eigenvalue problem yields a set of positive modes P^+ with wavenumbers k_z^+ and a set of negative modes P^- with wavenumbers k_z^-. The systematic ordering of the eigensolutions for ducts of arbitrary cross-section is not straightforward, particularly when many propagating modes are present. For example, the descriptor (m,n) which defines a mode by its radial order m and azimuthal order n ((22, 1) say for the first radial mode of azimuthal order 22) is only meaningful for axisymmetric ducts with axisymmetric liners. In the current study a general approach is adopted whereby modes are ordered on the basis of their cut-on ratio

$$\eta = |\sqrt{1 - [M_0 + (1 - M_0^2)k_z/k]^2}|, \tag{10}$$

this being defined in the usual way so that $\eta = 1$ corresponds to the transition from a propagating to an evanescent mode in a hard-walled duct. In a lined duct there is no sudden transition, but the cut-on ratio is still a strong indicator of whether a mode contributes significantly to acoustic power in the duct.

For lined duct with flow, one of the surface waves can be considered as an instability [5], although there is some debate as to whether this classification is mathematically correct [9]. Therefore it needs to be dealt with separately as the criteria used above for the acoustic modes does not apply.

In addition, when non-uniform flow is present the eigenvalue problem (7) also yields hydrodynamic modes which are convected with the mean flow. Some of these may also be unstable and correspond to Kelvin–Helmholtz instabilities of the mean flow profile. This case is not considered in the present paper, and results are presented for uniform mean flows only.

2.4. Results and validation

To validate the numerical eigenvalue solver, an axisymmetric problem is considered so as to compare with exact solutions given by analytic methods. The duct is annular with inner radius $R_1 = 0.7\,\mathrm{m}$ and outer radius $R_0 = 1\,\mathrm{m}$. The specific impedance is $Z = 2 - \mathrm{i}$ for the inner wall and $Z = 2 + \mathrm{i}$ for the outer wall (the specific impedance is non-dimensional with respect to the local values of density and sound speed). The mean flow is uniform with Mach number $M_0 = 0.4$, local sound speed $340\,\mathrm{m/s}$ and local density $1.23\,\mathrm{kg/m^3}$. The Helmholtz number is $kR_0 = 15$. The analytical values of the wavenumbers are obtained by solving the characteristic equation of the problem using a tracking method originally proposed by Eversman [10] and recently refined by Rienstra [5]. The wavenumbers of the eigensolutions are tracked in the complex plane as the impedance is varied from a hard-walled case (where all possible values of the wavenumber are easily found) to the impedance of interest. Rienstra has further refined this technique by defining guidelines so as to find all possible eigensolutions, including surface waves. The present implementation of this method is due to McAlpine et al. [11].

A series of structured and unstructured meshes with quadratic triangular elements is used to assess the influence of the mesh resolution on the accuracy of the numerical eigenvalues (examples of meshes are given in Fig. 2). The mesh resolution is characterized by a number of points per wavelength defined as $c_0/f/h$ where f is the frequency and h is the typical inter-nodal distance in a given mesh. The accuracy of the numerical model is assessed by considering the relative error on the axial wavenumber $|k_z - k_{z,ex}|/k$ where $k_{z,ex}$ is the exact value.

The relative error is plotted as a function of the cut-on ratio of the modes and for different mesh resolutions in Figs. 3 and 4 for structured and unstructured meshes. As a general trend, the error grows with the cut-on

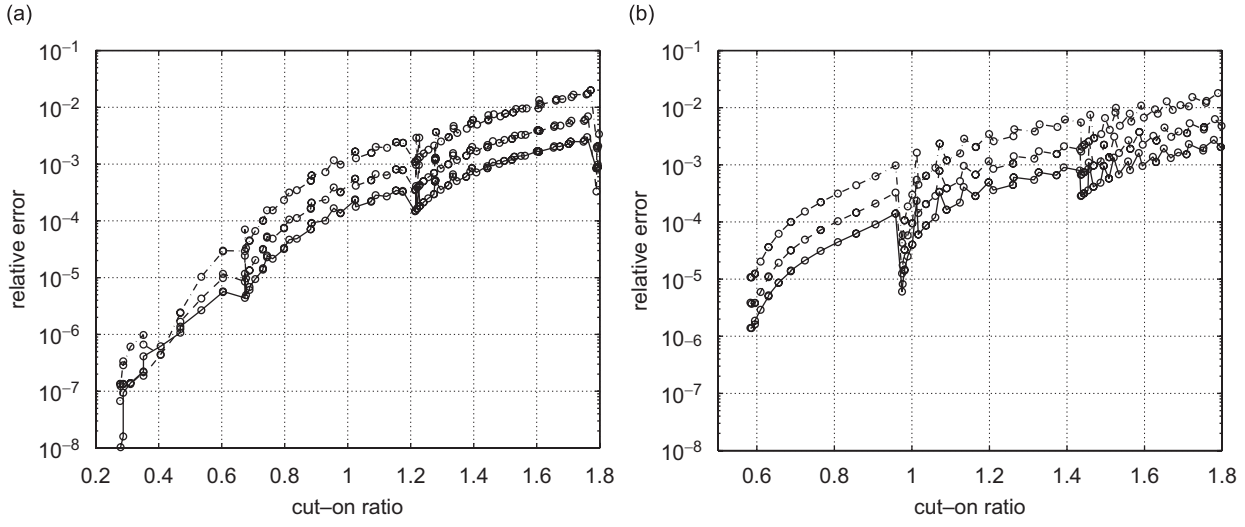

Fig. 3. Relative error on the wavenumbers with structured meshes for (a) the positive modes and (b) the negative modes. Mesh resolution is 12.9 (dot-dashed line), 17.3 (dashed line) and 21.6 (solid line) points per wavelength.

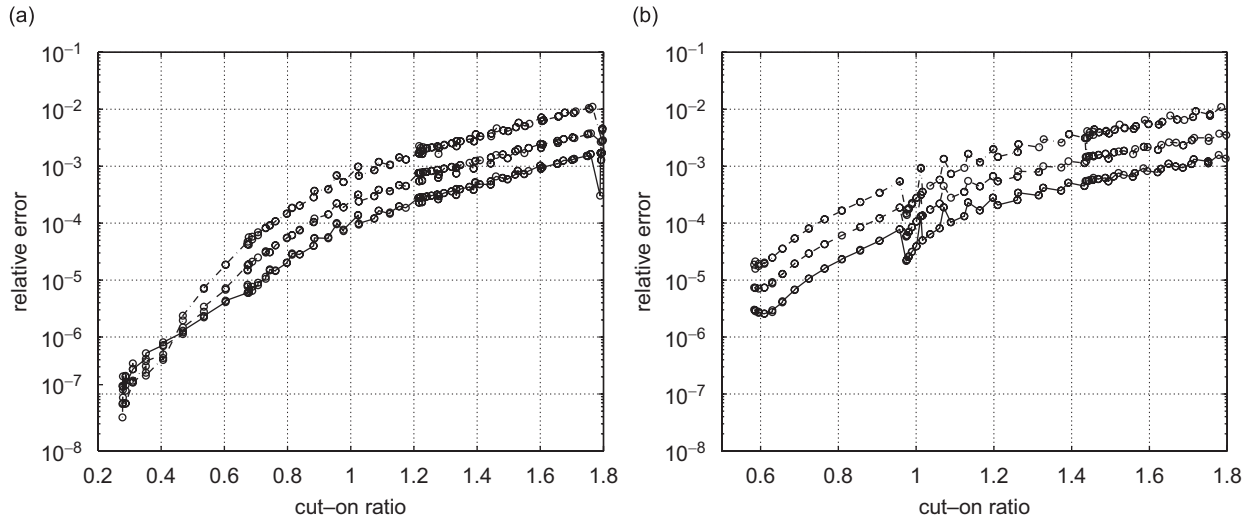

Fig. 4. Relative error on the wavenumbers with unstructured meshes for (a) the positive modes and (b) the negative modes. Mesh resolution is 13.6 (dot-dashed line), 17.4 (dashed line) and 22 (solid line) points per wavelength.

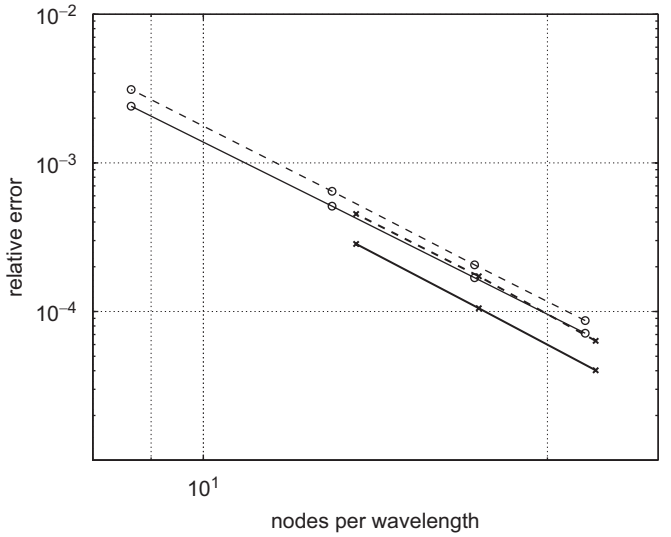

Fig. 5. Convergence of the numerical wavenumber with the mesh resolution for a positive mode (solid line) and a negative mode (dashed line). Structured meshes: thin lines; unstructured meshes: thick lines.

ratio of the mode. This is obviously due to the fact that the mode shapes of higher order modes are more complex and less accurately resolved on the FE meshes. For well cut-on modes, very accurate results can be obtained with relatively coarse meshes. Furthermore, for all the modes the numerical error is also consistently reduced when the mesh resolution is increased. This is shown more clearly in Fig. 5 where the relative error for a particular mode is plotted against the number of points per wavelength. The numerical wavenumber converges smoothly to the exact value with a fourth-order rate of convergence. In Fig. 3, it can be noted that with structured meshes the numerical error can vary significantly from one mode to the next. This is due to the fact that for some modes the azimuthal symmetry of the mesh matches that of the mode. As one might expect, this effect is less pronounced with unstructured meshes.

3. Mode matching at liner discontinuities

Modal scattering can be modelled at the interface between two prismatic sections with different circumferential liner distributions by matching modal expansions across the liner discontinuity. The numerical eigensolutions described in the preceding section form the modal expansions in each duct segment. The matching conditions are obtained from a variational statement for the field equations and impedance boundary condition over a vanishingly small control volume which includes the liner discontinuity. This gives a finite contribution to the matching conditions from the bounding contour of this interface for a non-zero axial slip velocity at the lined wall. This contribution has been neglected in previous mode-matching schemes, but has a discernible effect on the matched solution, particularly on the reflected components.

3.1. Formulation of the problem

Consider a prismatic duct composed of several axial segments of finite length, see Fig. 1. These have the same cross-section but different circumferentially varying impedances. We seek to establish appropriate matching conditions for solutions on either side of an interface between two such sections. Initially we will assume that the axial change in liner impedance occurs over a finite distance $\pm\varepsilon$ on either side of the matching plane at $z=0$ as indicated in Fig. 6. Matching conditions will be established for this finite transition region and the limit taken as $\varepsilon \to 0$ to simulate an abrupt discontinuity at $z=0$. The cross-section of the duct at $z=0$ defines an area S bounded by a contour Γ. In regions (1) and (2) on either side of the transition region, the complex acoustic pressure and cartesian velocity amplitudes are taken to be p_1, u_1, v_1, and w_1 for $z \leqslant -\varepsilon$, and p_2, u_2, v_2 and w_2 for $z \geqslant -\varepsilon$. These solutions can be written as modal expansions in each region. The acoustic pressure amplitudes, p_1 and p_2, for example, can be approximated by truncated series:

$$p_1(x,y,z) = \sum_{\alpha=1}^{N} [A^+_{1,\alpha} \mathrm{e}^{-\mathrm{i}k^+_{1,\alpha}z} P^+_{1,\alpha}(x,y) + A^-_{1,\alpha} \mathrm{e}^{-\mathrm{i}k^-_{1,\alpha}z} P^-_{1,\alpha}(x,y)] \quad \text{with } z < -\varepsilon, \tag{11}$$

$$p_2(x,y,z) = \sum_{\alpha=1}^{N} [A^+_{2,\alpha} \mathrm{e}^{-\mathrm{i}k^+_{2,\alpha}z} P^+_{2,\alpha}(x,y) + A^-_{2,\alpha} \mathrm{e}^{-\mathrm{i}k^-_{2,\alpha}z} P^-_{2,\alpha}(x,y)] \quad \text{with } z > \varepsilon, \tag{12}$$

where $A^{\pm}_{m,\alpha}$, are modal coefficients, $k^{\pm}_{m,\alpha}$ are axial wavenumbers and $P^{\pm}_{m,\alpha}$ are transverse eigenfunctions in regions (1) and (2). Note that the modes are numbered with a single index α. The more usual arrangement of numbering modes by using separate azimuthal and radial orders is not applicable when the impedance varies around the duct perimeter and the modes are no longer separable in r and θ. In the current scheme the index α is obtained by ranking the modes on the basis of the cut-on ratio (10).

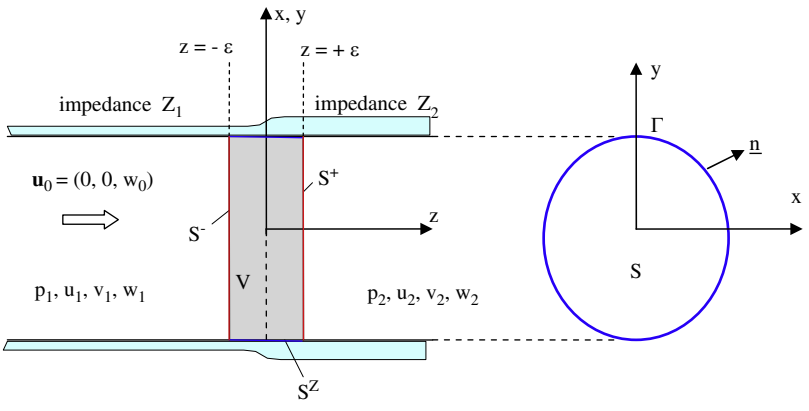

Fig. 6. Matching at a liner discontinuity, geometry and control volume.

3.2. The matching scheme

At all points within the duct, and specifically in matching region ($-\varepsilon<z<\varepsilon$), the pressure and velocity amplitudes, $p(\mathbf{x})$ and $\mathbf{u}(\mathbf{x})$, of the acoustic disturbance satisfy the time harmonic linearized momentum and continuity equations for inviscid, parallel flow:

$$\mathrm{i}\omega\mathbf{u} + w_0\frac{\partial\mathbf{u}}{\partial z} + \frac{1}{\rho_0}\nabla p = \mathbf{0} \quad \text{(momentum)},$$

$$\mathrm{i}\omega p + w_0\frac{\partial p}{\partial z} + \rho_0 c_0^2\nabla\cdot\mathbf{u} = 0 \quad \text{(continuity)}.$$

Here, $w_0(\mathbf{x}), c_0$ and ρ_0 denote the axial velocity, sound speed and density of the mean flow. c_0 and ρ_0 are constant over the duct cross-section. In formulating the matching conditions we consider only the axial momentum equation and the continuity equation, and write these in 'conservation' form as

$$\mathrm{i}\omega u + \nabla\cdot\left(0, 0, w_0 w + \frac{1}{\rho_0}p\right) = 0, \tag{13}$$

$$\mathrm{i}\omega p + \nabla\cdot(\rho_0 c_0^2 u, \rho_0 c_0^2 v, w_0 p + \rho_0 c_0^2 w) = 0, \tag{14}$$

where $\mathbf{u}(\mathbf{x})$ has components (u, v, w). We consider solutions of these equations within a region V, bounded by the planes S^- and S^+ at $z = \pm\varepsilon$, and bounded also by a portion of the cylindrical duct wall denoted by S^z. The impedance boundary condition on S^z is given by

$$\mathbf{u}\cdot\mathbf{n} = Ap - \frac{\mathrm{i}w_0}{\omega}\frac{\partial(Ap)}{\partial z} \quad \text{on } S^z, \tag{15}$$

where the admittance is given by $A = 1/Z$. The impedance and the associated admittance are not specified precisely on S^z but vary continuously so that $Z = Z_1$ at $z = -\varepsilon$ and $Z = Z_2$ at $z = +\varepsilon$. The acoustic pressure and normal velocity are continuous at the upstream and downstream boundaries of the control region so that

$$p = p_1, \quad w = w_1 \quad \text{on } S^-, \tag{16}$$

$$p = p_2, \quad w = w_2 \quad \text{on } S^+. \tag{17}$$

Eqs. (13) and (14) are now multiplied by a continuous weighting function $W(x, y)$ and integrated over V. Green's theorem is applied to the resulting integrals in the usual way and boundary conditions (15)–(17) are substituted in the resulting integral statement. This yields a variational formulation which states that any solution of Eqs. (13) and (14) in V which satisfies conditions (15)–(17) on its boundary, satisfies also the integral statements that

$$\int_V (\mathrm{i}\omega\overline{W}w)\,\mathrm{d}V + \int_{S^+}\overline{W}\left(w_0 w_2 + \frac{1}{\rho_0}p_2\right)\mathrm{d}S - \int_{S^-}\overline{W}\left(w_0 w_1 + \frac{1}{\rho_0}p_1\right)\mathrm{d}S = 0 \tag{18}$$

and

$$\int_V (\mathrm{i}\omega\overline{W}p)\,\mathrm{d}V + \int_{S^+}\overline{W}(w_0 p_2 + \rho_0 c_0^2 w_2)\,\mathrm{d}S - \int_{S^-}\overline{W}(w_0 p_1 + \rho_0 c_0^2 w_1)\,\mathrm{d}S + \int_{S^z}\rho_0 c_0^2\overline{W}\left[Ap - \frac{\mathrm{i}w_0}{\omega}\frac{\partial}{\partial z}(Ap)\right]\mathrm{d}S = 0, \tag{19}$$

for all admissible (i.e. continuous) test functions $W(x, y)$. To obtain the correct matching condition across a liner discontinuity we take the limit of the above expressions as $\varepsilon \to 0$. In doing so, we assume that p and w are finite or have weak singularities of order $r^{-1/2}$ on Γ. This ensures that the integrals over V in the above equations vanish as $\varepsilon \to 0$. Statement (18) then gives

$$\int_S w_0\overline{W}(w_2 - w_1)\,\mathrm{d}S + \int_S\frac{1}{\rho_0}\overline{W}(p_2 - p_1)\,\mathrm{d}S = 0. \tag{20}$$

Eq. (19) must be treated more carefully. The final integral is first rewritten as

$$\int_{S^\varepsilon}\left[\rho_0 c_0^2 \overline{W} A p - \frac{\partial}{\partial z}\left(\frac{\mathrm{i} w_0 \rho_0 c_0^2}{\omega}\overline{W} A p\right)\right]\mathrm{d}S$$

and the second term is integrated explicitly in z to give

$$\int_{S^\varepsilon} -\frac{\partial}{\partial z}\left[\frac{\mathrm{i} w_0 \rho_0 c_0^2}{\omega}(\overline{W} A p)\right]\mathrm{d}S = -\int_{\Gamma^+}\frac{\mathrm{i} w_0 \rho_0 c_0^2}{\omega}(\overline{W} A_2 p_2)\,\mathrm{d}\Gamma + \int_{\Gamma^-}\frac{\mathrm{i} w_0 \rho_0 c_0^2}{\omega}(\overline{W} A_1 p_1)\,\mathrm{d}\Gamma,$$

where $\Gamma^\pm$ are contours along the perimeter of the duct at $z = \pm\varepsilon$. When this is substituted into expression (18) and the limit taken as $\varepsilon \to 0$, we obtain

$$\int_S \rho_0 c_0^2 \overline{W}(w_2 - w_1)\,\mathrm{d}S + \int_S w_0 \overline{W}(p_2 - p_1)\,\mathrm{d}S = \int_\Gamma \frac{\mathrm{i} w_0 \rho_0 c_0^2}{\omega}\overline{W}(A_2 p_2 - A_1 p_1)\,\mathrm{d}\Gamma. \tag{21}$$

Eqs. (20) and (21) are the correct weighted conditions for matching acoustic solutions across an axial liner discontinuity at $z = 0$. Some special cases are of particular interest.

3.2.1. Zero mean flow

In the absence of flow ($w_0 = 0$) the term on the right-hand side of Eq. (21) vanishes and it is not difficult to show that conditions (20) and (21) reduce to

$$\int_S \overline{W}(p_2 - p_1)\,\mathrm{d}S = 0 \quad \text{and} \quad \int_S \overline{W}(w_2 - w_1)\,\mathrm{d}S = 0.$$

These impose continuity of pressure and normal velocity over the duct area S in a conventional 'weighted residual' sense without reference to the impedance boundary condition. These are the matching conditions which are in use currently in most mode-matching schemes with and without flow.

3.2.2. Uniform mean flow

When the flow in the duct is uniform, the axial flow velocity w_0 can be removed from the integrals over S. It is then not difficult to show that expressions (20) and (21) reduce to

$$\int_S \overline{W}(p_2 - p_1)\,\mathrm{d}S = -\frac{\mathrm{i} M_0^2}{1 - M_0^2}\frac{\rho_0 c_0^2}{\omega}\int_\Gamma \overline{W}(A_2 p_2 - A_1 p_1)\,\mathrm{d}\Gamma, \tag{22}$$

$$\int_S \overline{W}(w_2 - w_1)\,\mathrm{d}S = \frac{\mathrm{i} M_0}{1 - M_0^2}\frac{c_0}{\omega}\int_\Gamma \overline{W}(A_2 p_2 - A_1 p_1)\,\mathrm{d}\Gamma. \tag{23}$$

The presence of non-zero terms on the right-hand side of these expressions shows that integrable singularities of acoustic pressure can occur at impedance discontinuities when flow is present, and must be taken into account when solutions are matched across such interfaces. A similar surface contribution to the integrated energy flux has been identified by Eversman in an analysis of the acoustic power in a lined flow duct and shown to make a small but significant contribution to the total acoustic power [12,13].

As illustrated by the present analysis and also by the results to be presented in Section 3.5, the behaviour of the acoustic field at the liner discontinuity is particularly important. Rienstra and Peake have solved the problem of the transition from hard to soft wall in a circular duct with uniform flow [14,15]. Their analysis shows that the use of a Kutta or no-Kutta condition at the discontinuity can affect significantly the modal scattering. It was also found that the causality of the solution and the existence of an unstable hydrodynamic surface wave are directly related to the Kutta condition.

A related issue is the choice of the variables used to represent the acoustic field (see for instance Ref. [16]). The nature of the singularity observed at the liner discontinuity is different depending on the acoustic variable being pressure, velocity potential, etc. Using pressure and velocity in the standard matching conditions implies that these quantities are sufficiently well behaved to apply the matching, this assumption might in turn constrain the behaviour of the acoustic solution at the liner discontinuity. Although how one should model this transition is still an open question, one should note that the present method based on the conservation of

mass and momentum is clearly more general than the standard approach using continuity of acoustic pressure and velocity.

Unfortunately, there is as yet no definite and complete description of the physical mechanisms taking place at the transition from hard to soft surfaces with flow. And to make matters worse, the physical processes involved in such a transition are likely to be different if the liner is a porous material or a set of Helmholtz resonators behind a perforated sheet.

3.3. Application to modal solutions

Modal solutions are matched across a liner discontinuity by substituting truncated modal expansions (11) and (12) into expressions (22) and (23). This gives a set of algebraic equations

$$\mathbf{X}\begin{pmatrix}\mathbf{A}_2^+\\ \mathbf{A}_1^-\end{pmatrix}=\mathbf{Y}\begin{pmatrix}\mathbf{A}_1^+\\ \mathbf{A}_2^-\end{pmatrix}, \tag{24}$$

with

$$\mathbf{X}=\begin{bmatrix}\mathbf{P}_2^+ & -\mathbf{P}_1^-\\ \mathbf{M}_2^+ & -\mathbf{M}_1^-\end{bmatrix},\quad \mathbf{Y}=\begin{bmatrix}\mathbf{P}_1^+ & -\mathbf{P}_2^-\\ \mathbf{M}_1^+ & -\mathbf{M}_2^-\end{bmatrix},$$

and where the sub-matrices $\mathbf{M}_{1,2}^{\pm}$ and $\mathbf{P}_{1,2}^{\pm}$ have components

$$(\mathbf{M}_n^{\pm})_{\alpha,\beta}=\int_S\left(w_0+c_0^2\frac{k_{z,n,\beta}^{\pm}}{\omega-w_0k_{z,n,\beta}^{\pm}}\right)\overline{W}_\alpha P_{n,\beta}^{\pm}\,\mathrm{d}S-\int_\Gamma\frac{\mathrm{i}w_0\rho_0c_0^2}{\omega}\overline{W}_\alpha A_n P_{n,\beta}^{\pm}\,\mathrm{d}\Gamma\quad\text{with } n=1,2,$$

$$(\mathbf{P}_n^{\pm})_{\alpha,\beta}=\int_S\frac{\omega\overline{W}_\alpha P_{n,\beta}^{\pm}}{\rho_0(\omega-w_0k_{z,n,\beta}^{\pm})}\,\mathrm{d}S\quad\text{with } n=1,2.$$

The choice of the trial function W_α is important. One possibility is to use the modes of the corresponding hard-wall duct. Although these modes form an orthogonal basis, it was found that this choice of trial functions leads to poorly conditioned matrices $\mathbf{X}$ which in turn render the solutions of Eq. (24) inaccurate. It is preferable to use different trial functions for $\mathbf{M}_n^{\pm}$ and $\mathbf{P}_n^{\pm}$ so as to maximize the conditioning of the matrices on the diagonal of $\mathbf{X}$ (namely $\mathbf{P}_2^+$ and $\mathbf{M}_1^-$). This is achieved by using $P_{2,\beta}^+$ and $P_{1,\beta}^-$ as trial functions for $\mathbf{P}_n^{\pm}$ and $\mathbf{M}_n^{\pm}$, respectively.

The matrices $\mathbf{X}$ and $\mathbf{Y}$ are calculated using the FE approximations of the mode shapes and wavenumbers. Compared to the eigenvalue analysis the matching requires only a small fraction of the computational resources used to solve the eigenvalue problems (7) and (8).

3.4. Implementation for multiple segments

For a duct composed of several sections, one must concatenate a number of matching conditions of type (24), one for each liner discontinuity. Consider for instance a duct composed of three sections with an inlet plane at $z=z_1$, an exhaust plane at $z=z_3$ with two internal liner interfaces at $z=z_{12}$ and $z=z_{23}$. In this case, two linear systems of equations similar to Eq. (24) must be included in the model. These are:

$$\mathbf{X}_{12}\begin{pmatrix}\mathbf{E}_2^+(z_{12})\mathbf{A}_2^+\\ \mathbf{E}_1^-(z_{12})\mathbf{A}_1^-\end{pmatrix}=\mathbf{Y}_{12}\begin{pmatrix}\mathbf{E}_1^+(z_{12})\mathbf{A}_1^+\\ \mathbf{E}_2^-(z_{12})\mathbf{A}_2^-\end{pmatrix}, \tag{25}$$

$$\mathbf{X}_{23}\begin{pmatrix}\mathbf{E}_3^+(z_{23})\mathbf{A}_3^+\\ \mathbf{E}_2^-(z_{23})\mathbf{A}_2^-\end{pmatrix}=\mathbf{Y}_{23}\begin{pmatrix}\mathbf{E}_2^+(z_{23})\mathbf{A}_2^+\\ \mathbf{E}_3^-(z_{23})\mathbf{A}_3^-\end{pmatrix}, \tag{26}$$

where Eq. (25) corresponds to the interface between Sections 1 and 2, and Eq. (26) corresponds to the interface between Sections 2 and 3. The amplitudes $\mathbf{A}_n^{\pm}$ as defined in Eqs. (11) and (12) represent the modal pressure

amplitudes at $z = 0$. But the interfaces are located at $z = z_{12}$ and $z = z_{23}$. So we have introduced the matrices $\mathbf{E}_n^{\pm}(z)$ to account for the propagation of the modes along the duct. These diagonal matrices are defined by

$$(\mathbf{E}_n^{\pm}(z))_{\alpha\alpha} = \exp(-\mathrm{i}k_{z,n,\alpha}^{\pm} z).$$

The linear equations (25) and (26) are not solved directly for the mode amplitudes $\mathbf{A}_n^{\pm}$ since these algebraic systems are generally ill conditioned. This stems from the fact that the coefficients in the matrix $\mathbf{E}_n^{\pm}(z)$ can be either very large or very small depending on the imaginary part of the mode wavenumbers. This results in $\mathbf{E}_n^{\pm}(z)$ being close to singular and a direct inversion of Eqs. (25) and (26) is either impossible or prone to round-off error. A standard iterative method is used to avoid this problem [17].

The solution of the linear systems Eqs. (25) and (26) gives the scattering matrix $\mathbf{D}$ of the duct defined by the relationship

$$\begin{pmatrix} \mathbf{A}^- \\ \mathbf{B}^+ \end{pmatrix} = \mathbf{D} \begin{pmatrix} \mathbf{A}^+ \\ \mathbf{B}^- \end{pmatrix} \quad \text{with } \mathbf{D} = \begin{bmatrix} \mathbf{D}_{AA} & \mathbf{D}_{AB} \\ \mathbf{D}_{BA} & \mathbf{D}_{BB} \end{bmatrix}, \tag{27}$$

where $\mathbf{A}^{\pm}$ are the mode amplitude at the duct inlet while $\mathbf{B}^{\pm}$ denote the mode amplitudes at the exhaust.

3.5. Results and validation

To validate the FE mode-matching scheme, it is tested against ACTRAN, a commercial code for flow acoustics [18]. The test case used for this comparison is an annular duct composed of three 1 m long segments. The inner and outer radii of the duct are $R_1 = 0.7$ m and $R_0 = 1$ m, respectively. The first and third segments have hard walls while the second segment is lined with a specific impedance $Z = 2 + \mathrm{i}$ on the outer wall and $Z = 2 - \mathrm{i}$ on the inner wall. The flow Mach number is $M_0 = 0.4$. The fluid stagnation sound speed and density are 340 m/s and 1.23 kg/m^3. The Helmholtz number is $kR_0 = 15$. The problem being axisymmetric, it is possible to obtain a reference solution for the 3-D problem by using ACTRAN with a high resolution axisymmetric FE mesh.

First, the benefit of using the modified matching conditions based on the conservation of mass and momentum is demonstrated. To that end the mode-matching model is used to predict the transmission loss (i.e. the acoustic power absorbed by the liner) which is generally the quantity of practical interest for engineering design of duct liners. A structured mesh with an average of 17.3 points per wavelength is used and 100 modes are included in the mode matching. For each incident mode at the duct inlet Fig. 7 shows the

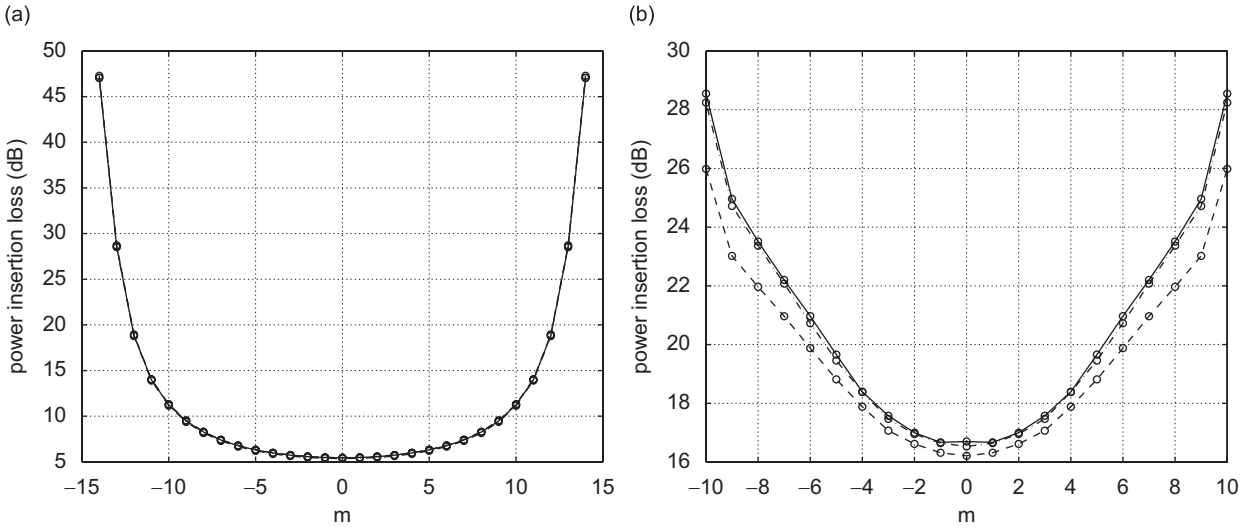

Fig. 7. Modal transmission loss for (a) the first-order radial modes and (b) the second-order radial modes. Solid line: reference solution. Dashed line: standard matching conditions. Dot-dashed line: modified matching conditions.

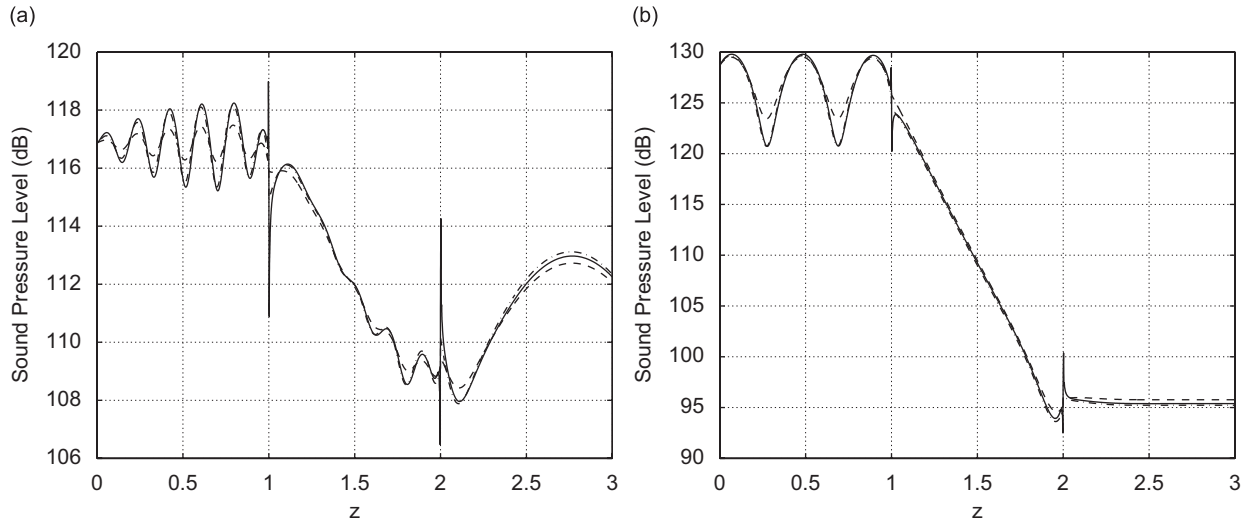

Fig. 8. Sound pressure level along the outer duct wall for (a) the plane wave and (b) the mode (13, 0). Solid line: reference solution. Dashed line: standard matching conditions. Dot-dashed line: modified matching conditions.

transmission loss given by the reference solution and by the standard and modified mode-matching schemes. While the modified matching scheme yield good results with an error remaining below half a decibel for all the modes, the standard matching condition based on the continuity of pressure and axial velocity exhibit relatively large error (more than 1 dB), especially for the higher order modes.

This issue is also clearly illustrated by comparing the pressure amplitude along the duct wall. In Fig. 8 the sound pressure level along the outer wall is plotted for two different incident modes, the plane wave and the mode (13, 0). Again the difference between the standard and modified matching is clearly visible. The results from the modified matching follow closely the reference solution whereas the pressure profile obtained with the standard matching deviates significantly from the reference solution especially in the first segment where errors of more than 1 dB can be observed. A particular feature of the solutions is the discontinuity observed at the interfaces on both side of the line segment. In presence of flow, a discontinuity in impedance at the wall induces a singular pressure field in the vicinity of the discontinuity. This singular solution is reasonably well captured by the modified matching but the standard matching scheme is unable to resolve properly the behaviour of the solution in the vicinity of the interfaces.

The accuracy of the numerical mode-matching method is now assessed with respect to the number of modes used for the matching. The relative error on pressure along the outer wall $|p(z) - p_{ex}(z)|/|p_{ex}(z)|$ where $p_{ex}(z)$ is the reference solution, is calculated using the modified matching conditions, see Fig. 9. Again the plane wave and the mode (13, 0) are used as sources at the duct inlet. In each case only modes with the same azimuthal order as the source are used in the mode matching. The number of radial modes included in the matching is varied from 2 to 5 to assess the convergence of the method. The numerical error decreases consistently as more modes are included in the matching. Large errors are observed at the interfaces between the lined and hard-walled segments. The behaviour of the solution close to the interfaces is controlled by the amplitudes of the high-order modes. Since these modes are well cut-off and decay rapidly, their influence is limited to the vicinity of the interface and their contributions at the inlet and exhaust of the duct are negligible.

Fig. 9 represents a particularly stringent assessment of the numerical error since one is generally interested in the modal power at the duct exhaust using the dB scale. So a different assessment of the convergence is carried out by considering the error on the transmission loss, see Fig. 10. In this calculation all the modes obtained from the eigenvalue problem are included in the mode matching (that is all the azimuthal orders are included at the same time). There is a total of 50 cut-on modes for this test case and the number of modes included in the matching is varied from 100 to 50. It is observed that there is very little variation in the transmission loss as the number of modes included in the matching is reduced. In fact, even when only the

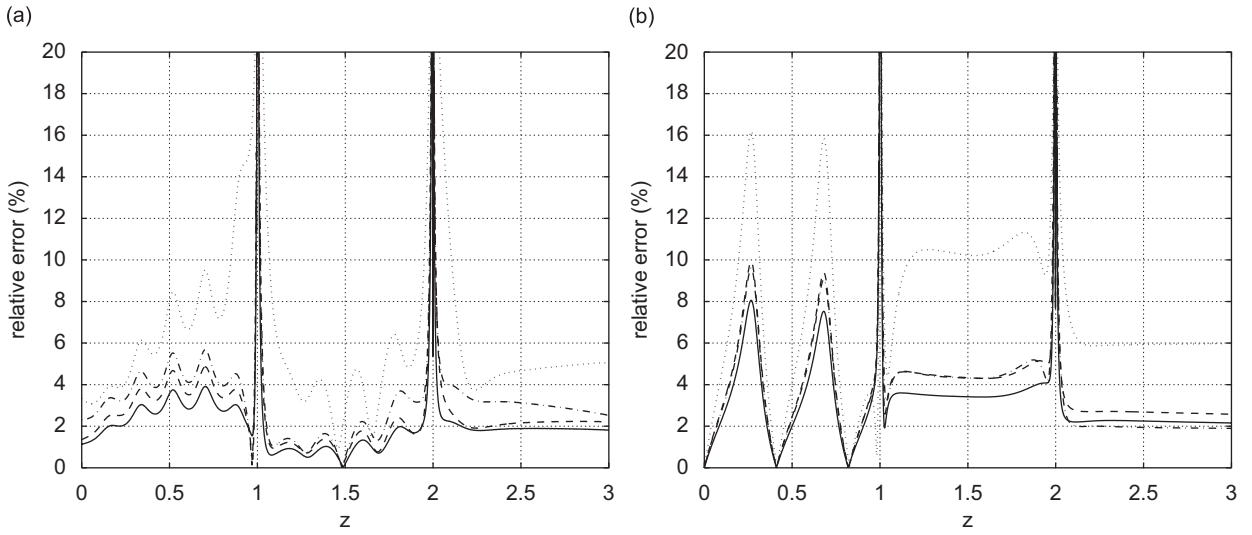

Fig. 9. Relative error on the complex pressure amplitude along the outer duct wall for (a) the plane wave and (b) the mode (13, 0). Number of modes included in the matching: 5 (solid line), 4 (dashed line), 3 (dot-dashed line), 2 (dotted line).

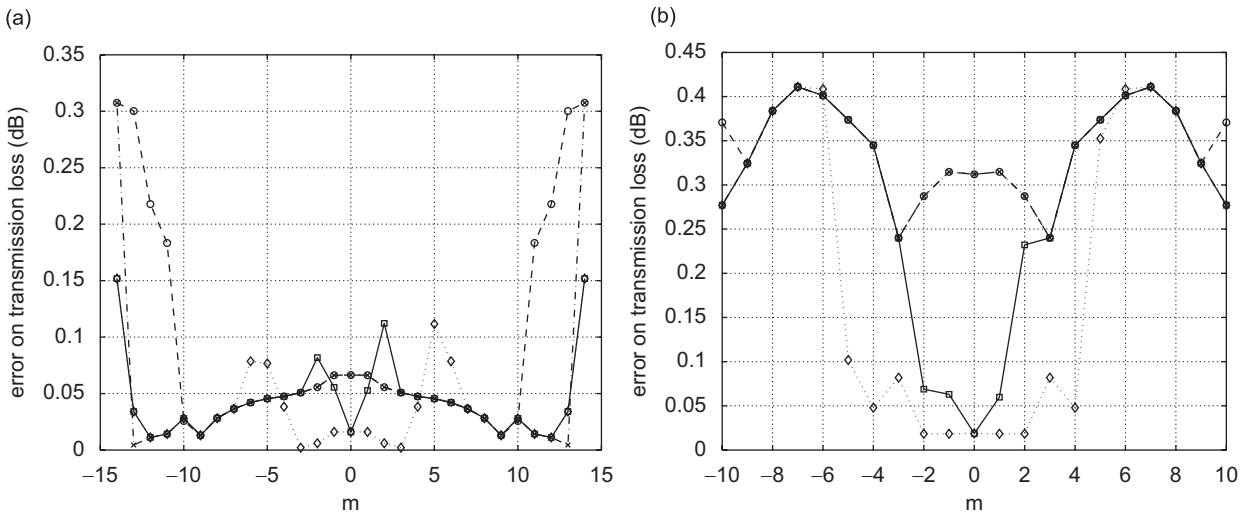

Fig. 10. Error on the modal transmission loss in dB for (a) the first-order radial modes and (b) the second-order radial modes. Number of mode included in the matching: 80 (dotted line), 70 (solid line), 60 (dot-dashed line) and 50 (dashed line).

cut-on modes are used the mode matching is able to predict the transmission within 0.5 dB. This demonstrates the robustness of the proposed FE mode-matching technique.

4. Noise radiation to the far field

Studies of liner performances are often limited to in-duct propagation and assess the power loss achieved by different liner configurations. But it is important to characterize these performances in terms of reduction of the noise radiated out of the duct to the far field. By integrating the mode-matching method with a radiation model, it is possible to obtain a simple engineering tool for investigating directly how the liner distribution influences the noise in the far field.

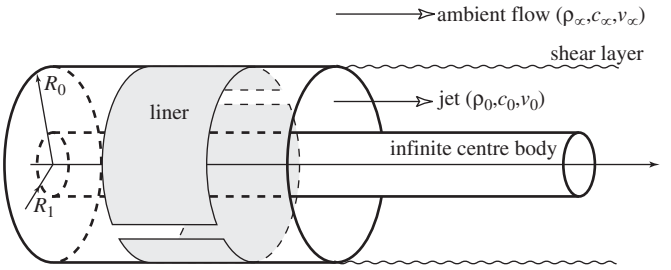

Fig. 11. The idealized model representing noise radiation from bypass ducts.

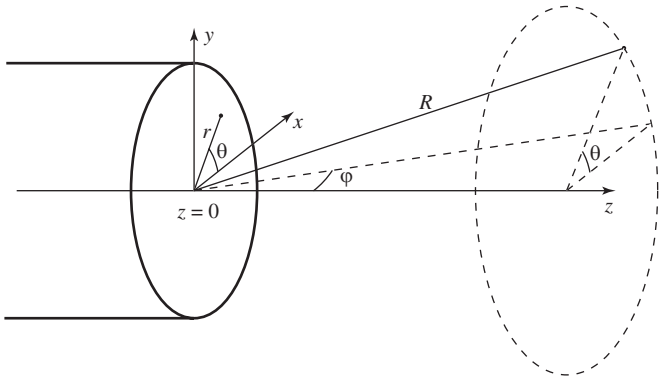

Fig. 12. Sketch of the duct together with the three coordinate systems used in this paper: cartesian coordinates (x, y, z), cylindrical coordinates (r, θ, z) and spherical coordinates (R, θ, φ).

The radiation model used in the present work is an analytic solution for the sound radiation from a semi-infinite jet pipe and it is an extension of the work by Munt [19,20] and Rienstra [21]. Only the main features of the model are outlined in this section, see Ref. [22] for technical details. The configuration, described in Fig. 11, is that of a semi-infinite circular duct with an infinite center body. The duct carries a jet described as a uniform, axial, steady flow with velocity w_0, sound speed c_0 and density ρ_0. The jet is surrounded by an ambient flow which is also a uniform, axial, steady flow but with different properties: velocity w_∞, sound speed c_∞ and density ρ_∞. The Mach number of the ambient flow is denoted $M_\infty = w_\infty/c_\infty$. For each normal mode of the duct, this analytic solution provides both the directivity functions in the far field and the reflection coefficients at the duct exhaust.

4.1. Far-field directivity

The sound radiated in the far field can be described as the sum of contributions from each outgoing mode B^+_{mn} at the duct exhaust. Each mode produces a different directivity patterns in the far field. It can be shown that the pressure in the far field reads (see Fig. 12 for a definition of the spherical coordinates)

$$p(R,\theta,\varphi) = \frac{1}{R}\sum_{m,n} B^+_{mn} D_{mn}(\varphi) \mathrm{e}^{\mathrm{i}\omega RS(\varphi)/c_0 + \mathrm{i}m\theta}, \tag{28}$$

where $D_{mn}(\varphi)$ is the directivity function of the mode (m,n) for a unit pressure mode amplitude. These directivity patterns depend on the duct geometry, the mode itself and the properties of the flow inside and outside the duct, in our case these are the jet properties (ρ_0, c_0, w_0) and ambient flow properties $(\rho_\infty, c_\infty, w_\infty)$. The factor $S(\varphi)$ accounts for the wavefront stretching introduced by the ambient mean flow:

$$S(\varphi) = \frac{\sqrt{1 - M_\infty^2 \sin^2\varphi} - M_\infty \cos\varphi}{1 - M_\infty^2}.$$

4.2. Reflection coefficients

As sound propagates out of the duct a part of the acoustic energy is reflected into the duct since there is a change in acoustic impedance at the duct exhaust plane. These reflections depends on the properties of the flow outside the duct and can be described by a reflection matrix $\mathbf{R}$ relating the reflected modes $\mathbf{B}^-$ to the outgoing modes $\mathbf{B}^+$:

$$\mathbf{B}^- = \mathbf{R}\mathbf{B}^+. \tag{29}$$

In practice the reflections at a bypass duct exhaust at operating conditions are marginal and can be neglected. This is due to the relatively high frequency and the high order of the modes considered ($kR = 30$ and $m = 26$ for instance).

4.3. Integration with the mode-matching method

To integrate the radiation model with the mode-matching method we assume that the duct is not lined at the exhaust plane. Although the numerical eigenvalue solver can be used to obtain the modes in a hard-wall section, it is preferable to derive these modes analytically in order to facilitate the integration with the radiation model. This is because, even for a hard-walled duct, the canonical modes $(+m, n)$ and $(-m, n)$ are not obtained directly with the numerical method. Instead it yields linear combinations of the modes $(+m, n)$ and $(-m, n)$ which makes the integration with the radiation model more difficult to implement.

The first step is to combine the scattering matrix of the duct with the reflection coefficients. By introducing Eq. (29) in Eq. (27), it is straightforward to derive

$$\mathbf{B}^+ = \mathbf{T}\mathbf{A}^+ \quad \text{with } \mathbf{T} = (\mathbf{I} - \mathbf{D}_{BB}\mathbf{R})^{-1}\mathbf{D}_{BA}, \tag{30}$$

where $\mathbf{T}$ is the transmission matrix of the duct and $\mathbf{I}$ denotes the identity matrix. While the scattering matrix depends solely on the duct properties, the transmission matrix depends also on the ambient flow since it takes the reflections at the duct exit into account.

4.4. Comments on the radiation model

An important aspect of radiation model is the presence of the vortex sheet separating the jet and the ambient flow. This vortex sheet emanates from the lip of the outer duct at $r = R_0$ and $z = 0$. The velocity potential can be discontinuous across the vortex sheet and this discontinuity represents vortices (with zero thickness) shed from the duct lip and convected by the mean flow. This mechanism of vorticity shedding is an additional degree of freedom of the system and it has to be specified by describing the behaviour of the solution at the duct edge (in mathematical terms, an edge condition is required so that the discontinuity of the solution across the vortex sheet is uniquely defined). This is the role of the Kutta condition which states that all the available vorticity is shed from the duct lip. In that case, the pressure is finite at the edge. The opposite situation is when no vorticity is shed from the duct lip. In that case, the pressure is singular but integrable at the edge. In practice, the situation is intermediate with only a limited amount of vorticity shed from the duct. In the results presented below, the Kutta condition is used since this is the most common edge condition used for exhaust problems. It is important to account properly for the vorticity shedding since it modifies the energy balance of the system and it acts either as a source or a sink of acoustic energy [23].

When the jet properties are different from that of the ambient flow, acoustic waves are refracted by the impedance mismatch across the vortex sheet. For exhaust problem, the acoustic energy is deviated away from the jet axis and this produces a cone of silence along the jet direction.

With a flow mismatch, a crucial issue is that the vortex sheet is unstable. An instability wave growing exponentially in the stream-wise direction is triggered by the acoustic waves. This instability wave represent the early growth of the shear layer. But its exponential growth is an artifact of the linear model used for the acoustic waves. In practice the instability waves is saturated by nonlinear effects which results in the formation of vortices and the growth of the shear layer thickness (an aspect which is also not included in the present model since the vortex sheet has a constant zero thickness). There is an ongoing debate on whether this linear

instability wave should be included in the solution [24,25]. The main argument for including the instability wave is that one has to include it in order to obtain a causal solution. Therefore, in the present work, the instability wave is included in the solution (yet it is not present in the far-field directivity function D_{mn} used in Eq. (28) as it is not a genuine acoustic field).

5. Application to bypass duct liners

The mode-matching method is now used to perform a parametric study of the influence of a hard patch on the wall of a lined bypass duct. Hard patches are small areas of a lined surface where the acoustic treatment has been removed either for design or for maintenance purposes. Hard patches can be due to the presence of other components of the engine that prevent the use of liner in some areas of the bypass duct. Maintenance also requires the removal of small parts of the liners which are then replaced by repair patches. Hard patches are detrimental to the performance of liners as they reduce the area of treated surfaces. They also introduce significant modal scattering by redistributing the acoustic energy onto low-order modes which are less attenuated.

Non-dimensional parameters are used for this test case with the outer radius of the duct, the local sound speed and density as reference values. To represent the bypass duct of a real engine, we consider a straight annular duct with hub-tip ratio 0.78 and length 3. The flow inside the duct is uniform with Mach number $M_0 = 0.447$. For the ambient flow, the Mach number is $M_\infty = 0.219$, the local density and local sound speed are 1.04 and 0.98. The duct is composed of three segments, see Fig. 13. The first and last segments have length 0.5 with hard walls. In the middle segment, the inner and outer walls of the duct are lined. The Helmholtz number is 15.7 and the liner specific impedance is $Z = 2 - \mathrm{i}$.

The mode-matching procedure is used to investigate the influence of the insertion of a rectangular hard patch on the outer wall of the middle segment as shown in Fig. 13. The area of the patch is kept constant and is taken to be 5% of the outer wall area in the middle segment. The aspect ratio of the patch is characterized by its width given in percent of the outer duct perimeter and is varied from 100% to 5%. With a width of 100% the patch is axisymmetric and is simply an extension of the first hard-walled segment. With 5% the patch is a narrow splice running all along the lined segment. The patch is centered on the upper half of the duct (i.e. it is located between $\theta = \pi/2 - \alpha$ and $\theta = \pi/2 + \alpha$ where α is the half-azimuthal width of the patch).

The mode amplitudes A^+_{mn} at the duct inlet represent the source of sound that will propagate in the duct and then radiate to the far field. These sound sources are generated by the fan blades and the outer guide vanes that are located just upstream of the bypass duct. Two categories of sources are generally considered for turbofan bypass ducts.

The first category comprises the tones generated by the fan blades and the rotor–stator interactions. These tones are best described as a well-defined set of modes at particular frequencies and azimuthal orders depending on the blade-passing frequency and the number of fan blades and guide vanes, see Ref. [26]. Therefore, this source is simply specified by the mode amplitudes A^+_{mn}.

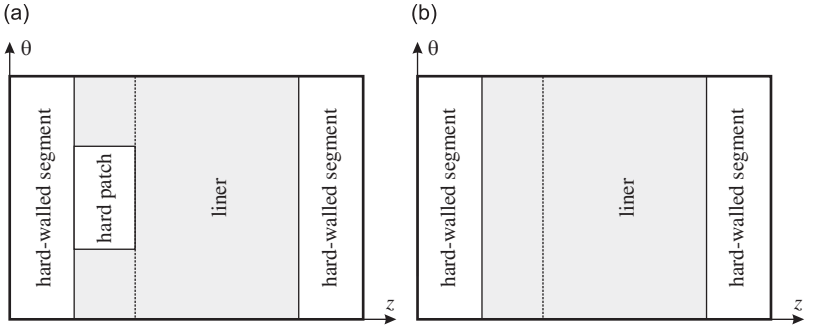

Fig. 13. Schematic of (a) the outer wall and (b) the inner wall of the bypass duct.

The second source of sound propagating in the bypass duct is the broadband noise generated by the interaction between the turbulence and the fan blades and the guide vanes. This produces broadband noise which is random and well distributed on the modes. To describe this type of noise, one has to consider the mode amplitudes A^+_{mn} as random variables and to specify their cross-correlation. A simple model commonly used for broadband noise is that of uncorrelated modes with equal modal power distribution. In that case, the correlation matrix is diagonal.

The problem at hand is completely specified when all the information described above is available: the definition of the source $\mathbf{A}^+$, the scattering matrix $\mathbf{D}$ of the duct, the reflection coefficients $\mathbf{R}$ and the directivity functions D_{mn}. It is then possible to calculate several results of interest such as the sound pressure level and acoustic intensity, in the far field and at the duct exit plane [27].

5.1. In-duct results

We first focus on the transmission properties of the duct. In Fig. 14 the effect of the hard patch is assessed by plotting the change in the total acoustic power due to the insertion of the hard patch. It is seen that the hard patch introduces a significant penalty on the efficiency of the acoustic treatment and that this penalty varies strongly with the patch aspect ratio. For the first radial modes, this effect is very important for modes with high azimuthal orders with insertion losses as high as 50 dB for modes close to cut-off. For the second radial modes, the modes with low azimuthal orders are the most affected by the hard patches with increases in total transmitted power varying between 8.5 and 13.5 dB.

Results in Fig. 14 are concerned with the total transmitted power and as such do not provide any information on the modal scattering introduced by the hard patch. Fig. 15 illustrates this modal scattering by plotting the modal power at the exhaust when the mode (10, 1) is used as an input at the duct inlet. Two patch widths, 5% and 25%, are shown. Although the incident mode is a second radial mode, the first radial modes are dominant at the duct exhaust, this is so because the second radial modes are more efficiently absorbed by the liner and the energy scattered onto the first radial modes is allowed to propagate with less attenuation. For the thin patch with width 5% the incident mode is scattered rather uniformly across the range of cut-on modes, but the modes $m = 10$ are still dominant. For the wide patch, the incident mode is scattered predominantly on modes whose azimuthal order is a multiple of 4. Having a width of 25% of the perimeter, the patch transfers the incident energy into modes having a similar symmetry.

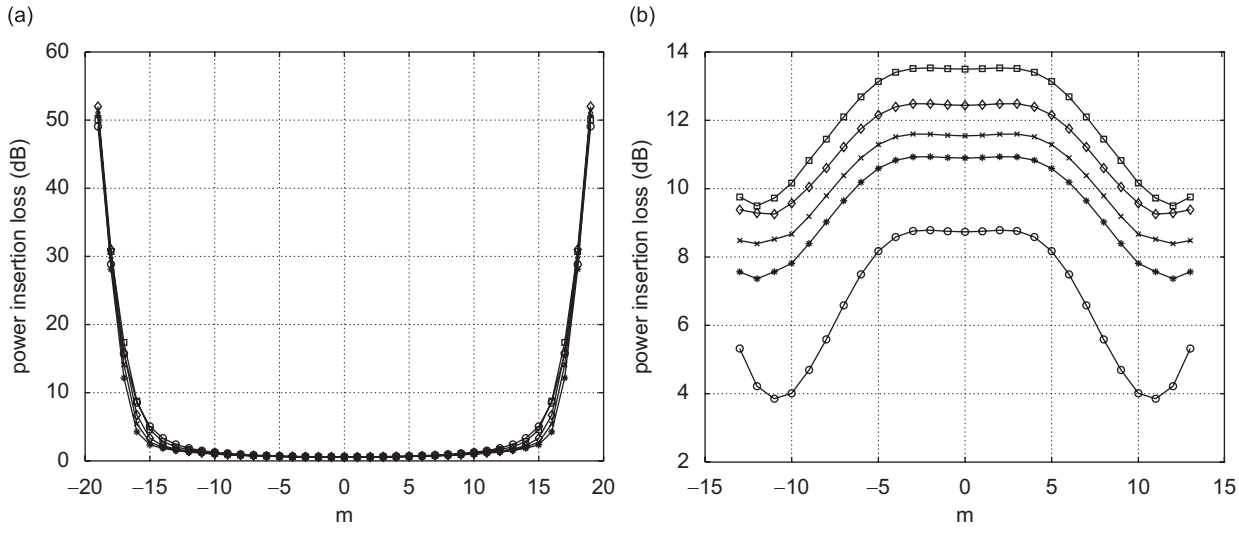

Fig. 14. Insertion loss in the total transmitted power in dB due to the hard patch for (a) the first radial modes and for (b) the second radial modes. The width of the patch is 10% (circles), 30% (squares), 50% (diamonds), 70% (crosses) and 90% (stars).

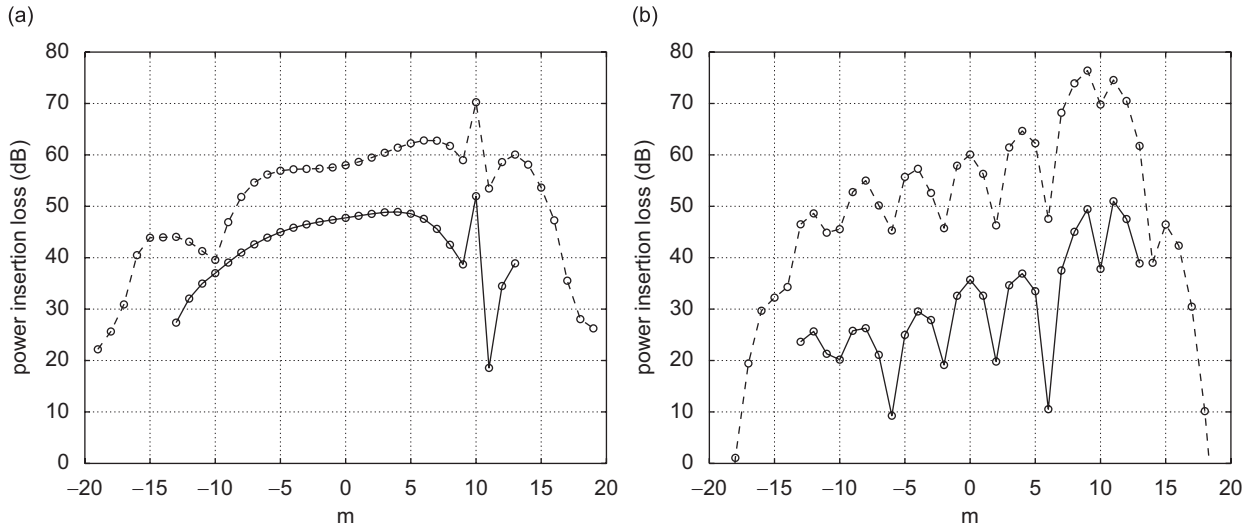

Fig. 15. Modal power at the duct exhaust with an incident mode (10, 1). (a) Patch width 5% and (b) Patch width 25%. Dashed line: first radial modes; solid line: second radial modes. The power of the incident mode is 120 dB.

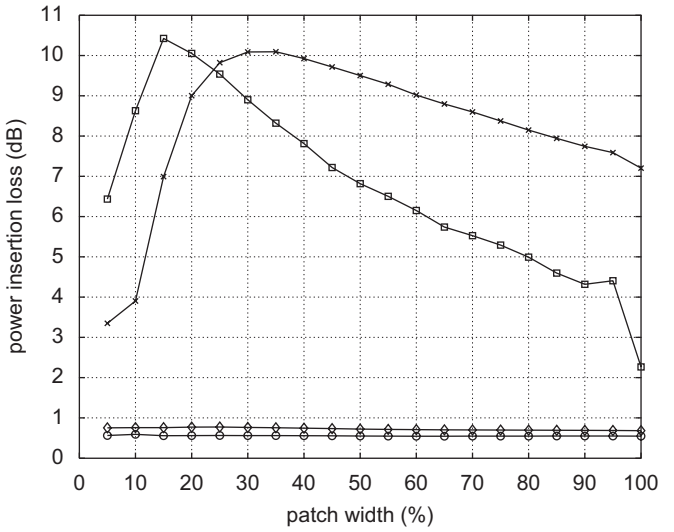

Fig. 16. Insertion loss of the hard patch for the total power radiated in the far field with the plane wave (○), the mode (10, 1) (×), the mode (16, 0) (□) and broadband noise (◇).

5.2. Far-field results

The effect of the hard patch is also assessed in terms of the noise radiated to the far field. Fig. 16 shows the change in the total acoustic power radiated to the far field due to the hard patch as a function of the patch width. For the plane wave the effect of the patch is marginal, the insertion loss being consistently below 0.5 dB. The liner having only a limited impact on the propagation of the plane wave, the presence of the hard patch does not introduce any significant scattering of the plane wave. For broadband noise, the effect of the hard patch is slightly larger but still below 1 dB and this is explained by the small fraction of the lined area removed by the hard patch. With broadband noise the sound field can be considered as a diffuse field. In that case sound absorption is directly proportional to the area covered by the liner and the modal scattering introduced

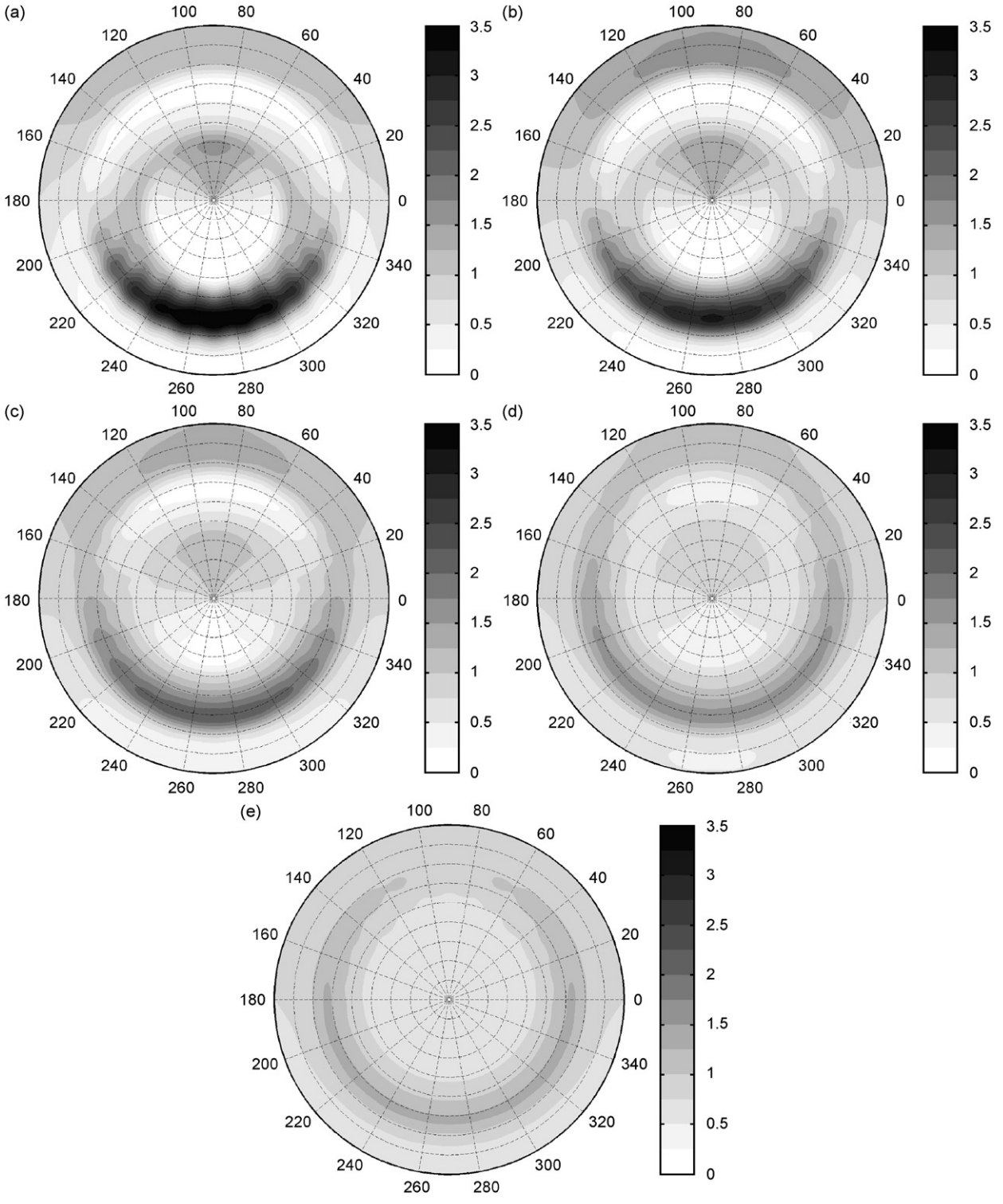

Fig. 17. Insertion loss for the acoustic intensity in the far field with broadband noise. The patch width is (a) 10%, (b) 30%, (c) 50%, (d) 70% and (e) 90%. In these graphs the intensity is plotted on the hemisphere of the rear arc viewed from some position downstream on the axis.

by the patch is of little importance. In contrast, the insertion loss for the mode (10, 1) is quite large with an increase of more than 10 dB for the patches of widths 30% and 35%. Interestingly, the configurations with narrow patches (5% and 10%) yield the smallest penalty with an increase of less than 4 dB of the total acoustic power. In fact, for this incident mode, a narrow patch is preferable over an axisymmetric one. The patch also has a large influence for the incident mode (16, 0) with an insertion loss above 10 dB for a 15% patch width. In that case however an axisymmetric or wide patch is clearly preferable to a narrow patch.

For broadband noise, the influence of the hard patch on the noise radiated to the far field is illustrated in more details in Fig. 17 by plotting the acoustic intensity in the rear arc. As shown in Fig. 16, for broadband noise the patch geometry has little effect on the total power radiated to the far field. It has however a significant impact on the directivity by modifying the distribution of acoustic energy in the far field. Wide patches are found to induce small and rather uniform increases in the acoustic intensity in the far field. In contrast, narrow patches increase significantly the acoustic intensity in the lower half of the directivity by as much as 3.5 dB. Obviously these liner configurations are particularly detrimental in terms of ground impact.

6. Conclusions and comments

In this paper a mode-matching procedure has been presented which is based on computed eigensolutions for ducts of arbitrary cross-section. The current matching procedure deals more accurately with impedance discontinuities and gives better correspondence with more detailed FE transmission analyses than do traditional mode-matching methods. The current approach is much less computationally demanding than full-scale three-dimensional transmission analyses and lends itself to parametric studies and to preliminary design evaluation of non-axisymmetric liner configurations.

Using the mode-matching method together with an analytic radiation model, the influence of non-axisymmetric liners can be characterized in terms of noise radiation to the far field. For applications to bypass duct problems, the radiation model includes the refraction of sound by the shear layer of the jet as well as the scattering by the afterbody of the turbofan. The results obtained show that the influence of non-axisymmetric liners on far-field directivity is far from simple and modal scattering at liner discontinuities can result in complex behaviour in terms of noise radiation.

This hybrid 'in-duct eigenmode + analytic radiation' model provides a practical tool for predicting far-field radiation patterns for 3D lined bypass ducts at frequencies and flow conditions of practical interest and including the effects of shear refraction in the external flow. It is currently being used as a basis for parametric and optimization studies to reduce the ground impact of aft-radiated noise by 3D liner placement.

Acknowledgements

The work reported in this article was supported by Rolls-Royce plc through the Rolls-Royce University Technology Centre in Gas Turbine Noise at the University of Southampton and also by the UK Department of Trade and Industry (DTI) through the NTAP[2] and ANDANTE[3] projects. The reference solutions of the eigenvalue problems were provided by Dr. Alan McAlpine and the ACTRAN simulations used for validating the mode-matching procedure were carried out by Dr. Rie Sugimoto.

References

[1] B. Regan, J. Eaton, Modelling the influence of acoustic liner non-uniformities on duct modes, *Journal of Sound and Vibration* 219 (5) (1999) 859–879.

[2] C. Fuller, Propagation and radiation of sound from flanged circular ducts with circumferentially varying wall admittances, *Journal of Sound and Vibration* 93 (3) (1984) 321–351.

[3] C. Fuller, R. Silcox, Experiments on sound radiation from a duct with a circumferentially varying liner, *AIAA Journal* 22 (6) (1984) 781–785.

[2]Noise Technology Acquisition Project (CARAD programme).

[3]Aircraft Noise Disturbance Alleviation by Novel Technology (DTI technology programme).

[4] W. Bi, V. Pagneux, Y. Auregan, Modelling of sound propagation in non-uniform lined duct using a multi-modal propagation method, *Journal of Sound and Vibration* 289 (2006) 1091–1111.
[5] S. Rienstra, A classification of duct modes based on surface waves, *Wave Motion* 37 (2003) 119–135.
[6] R. Astley, W. Eversman, A finite element formulation of the eigenvalue problem in lined ducts with flow, *Journal of Sound and Vibration* 65 (1) (1979) 61–74.
[7] R. Astley, The finite element duct eigenvalue problem: an improved formulation with Hermitian elements and no-flow condensation, *Journal of Sound and Vibration* 69 (1) (1980) 13–25.
[8] R. Lehoucq, D. Sorensen, C. Yang, *ARPACK Users' Guide: Solution of Large Scale Eigenvalue Problems with Implicitly Restarted Arnoldi Methods*, ⟨http://www.caam.rice.edu/software/ARPACK/index.html⟩.
[9] E. Brambley, N. Peake, Surface-waves, stability, and scattering for a lined duct with flow, *12th AIAA/CEAS Aeroacoustics Conference*, Boston, USA, 2006, AIAA paper 2006–2688.
[10] W. Eversman, Theoretical models for duct acoustic propagation and radiation, in: H.H. Hubbard (Ed.), *Aeroacoustics of Flight Vehicles: Theory and Practice*, Acoustical Society of America, 1995, pp. 101–163.
[11] A. McAlpine, R. Astley, V. Hii, N. Baker, A. Kempton, Acoustic scattering by an axially-segmented turbofan inlet duct liner at supersonic fan speeds, *Journal of Sound and Vibration* 294 (2006) 780–806.
[12] W. Eversman, Acoustic energy in ducts: further observations, *Journal of Sound and Vibration* 62 (4) (1979) 517–532.
[13] W. Eversman, Acoustic power in lined ducts, *10th AIAA/CEAS Aeroacoustics Conference*, 2004, AIAA paper 2004–2904.
[14] S. Rienstra, N. Peake, Modal scattering at an impedance transition in a lined flow duct, *11th AIAA/CEAS Aeroacoustics Conference*, Monterey, CA, 2005, AIAA paper 2005-2852.
[15] S. Rienstra, Acoustic scattering at a hard–soft lining transition in a flow duct, *Journal of Engineering Mathematics* 59 (2007) 451–475.
[16] E. Luneville, J.-F. Mercier, Finite element simulation of time-harmonic aeroacoustics with a generalized impedance boundary condition, *13th AIAA/CEAS Aeroacoustics Conference*, Rome, Italy, 2007, AIAA paper 2007–3483.
[17] A. Cummings, High frequency ray acoustics models for duct silencers, *Journal of Sound and Vibration* 221 (4) (1999) 681–708.
[18] Free Field Technologies, *Actran 2004 User's Manual*, Free Field Technologies, Louvain-la-Neuve, Belgium, 2004.
[19] R. Munt, The interaction of sound with a subsonic jet issuing from a semi-infinite cylindrical pipe, *Journal of Fluid Mechanics* 83 (4) (1977) 609–640.
[20] R. Munt, Acoustic transmission properties of a jet pipe with subsonic jet flow: I. The cold jet reflection coefficient, *Journal of Sound and Vibration* 142 (3) (1990) 413–436.
[21] S. Rienstra, Acoustic radiation from a semi-infinite annular duct in a uniform subsonic mean flow, *Journal of Sound and Vibration* 94 (2) (1984) 267–288.
[22] G. Gabard, R. Astley, Theoretical model for sound radiation from annular jet pipes: far- and near-field solutions, *Journal of Fluid Mechanics* 549 (2006) 315–341.
[23] S. Rienstra, Sound diffraction at a trailing edge, *Journal of Fluid Mechanics* 108 (1981) 443–460.
[24] A. Agarwal, P. Morris, Calculation of sound propagation in nonuniform flows: suppression of the instability waves, *AIAA Journal* 42 (1) (2004) 80–88.
[25] M. Goldstein, S. Leib, The role of instability waves in predicting jet noise, *Journal of Fluid Mechanics* 525 (2005) 37–72.
[26] J. Tyler, T. Sofrin, Axial flow compressor noise studies, *Society of Automotive Engineers Transactions* 70 (1962) 309–332.
[27] P. Joseph, C. Morfey, Multimode radiation from an unflanged, semi-infinite circular duct, *Journal of the Acoustical Society of America* 105 (5) (1999) 2590–2600.